Письма в ЭЧАЯ. 2001. №3[106] Particles and Nuclei, Letters. 2001. No.3[106]

УДК 539.123

RESULTS FROM THE AMANDA HIGH-ENERGY NEUTRINO DETECTOR

A.Biron

DESY-Zeuthen, D-15735, Zeuthen, Germany
For the AMANDA collaboration[1]

This paper briefly summarizes the search for astronomical sources of high-energy neutrinos using the AMANDA-B10 detector. The complete data set from 1997 was analyzed. For $E_\mu > 10$ TeV, the detector exceeds 10,000 m^2 in effective area between declinations of 25 and 90 degrees. Neutrinos generated in the atmosphere by cosmic ray interactions were used to verify the overall sensitivity of the detector. The absolute pointing accuracy and angular resolution have been confirmed by the analysis of coincident events between the SPASE air shower array and the AMANDA detector. Preliminary flux limits from point source candidates are presented. For declinations larger than +45 degrees, our results compare favorably to existing limits for sources in the Southern sky. We also present the current status of the searches for high-energy neutrino emission from diffusely distributed sources, GRBs, and WIMPs from the center of the Earth.

В работе приводятся обобщенные результаты исследования астрономических источников нейтрино высоких энергий с помощью детектора AMANDA-B10. Проанализированы экспериментальные данные, полученные с 1997 г. Для $E_\mu \gtrsim 10$ ТэВ эффективная площадь детектора превышает 10000 $м^2$ между склонениями 25 и 90°. Нейтрино, образующиеся в атмосфере под действием космических лучей, использовались для проверки полной чувствительности детектора. Точность направления и угловое разрешение были подтверждены анализом совпадающих событий между установкой по измерению атмосферных ливней SPASE и детектором AMANDA. Представлены предварительные результаты на пределы потока от точечных источников излучения. Для склонений больше, чем +45°, наши результаты находятся в хорошем соответствии с существующими пределами для источников южного небосклона. Также мы представляем текущее состояние нейтринного излучения высокой энергии от диффузно распределенных источников, вспышек гамма-излучения и слабо взаимодействующих массивных частиц в центре Земли.

INTRODUCTION

The AMANDA-B10 high-energy neutrino detector was constructed between 1500–2000 m below the surface of the Antarctic ice sheet where the optical properties are suitable for track reconstruction [1]. The instrumented volume forms a cylinder with outer diameter of 120 m. The surface electronics is located within a kilometer of the Amundsen–Scott Research Station at the geographic South Pole. The detector was commissioned in February 1997 [2,3], and initial scientific results were presented at the XXIV International Cosmic Ray Conference [1]. Reconstruction methods and detector calibration techniques are introduced in Ref. 4.

AMANDA-B10 consists of 302 optical modules (OMs), each containing an 8 inch diameter photomultiplier tube controlled by passive electronics which is housed in a glass pressure

[1]The full author list of the collaboration is given at the end of the paper.

vessel. They are connected to the surface by an electrical cable that provides high voltage and transmits the signals from the OM. The simple, reliable system architecture is responsible for the low fraction of OM failure (< 10 % after several years of operation, although most of the failures occur within a week after deployment).

In January 2000, AMANDA-II was completed. It consists of 19 strings with a total of 677 OMs arranged in concentric circles, with the ten strings from AMANDA-B10 forming the central core of the new detector. New surface electronics consolidates several triggering functions and adds functionality. New scalers were installed which provides millisecond resolution — important for Supernova studies. Several technologies were deployed to evaluate their utility and readiness for future expansion to larger systems.

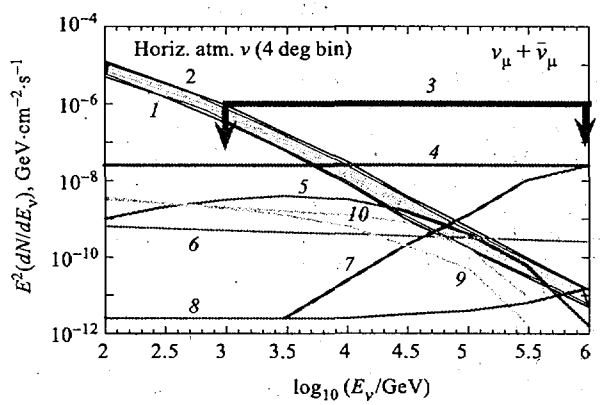

Fig. 1. Survey of $\nu + \bar{\nu}$ flux predictions from cosmic accelerators of high-energy neutrinos (adopted from the recent review by Learned and Mannheim [6]). The atmospheric neutrino fluxes are from [7], for both vertical (*1*) and horizontal (*2*) fluxes within a circle defined by a half angle of 4 degrees (labeled «4 deg bin»). The curves do not include the normalization uncertainty, possibly 20 % in magnitude. *3* — AMANDA-B10 limit reported here; *4* — Ref. 8 for the core emission from 3C273 due to *pp* interactions. It also represents neutrino emission from the AGN Blazar Mk501 during 1997 if it emits half of its TeV gamma ray flux in neutrinos; *5* — Crab Nebula, model I from [9]; *6* — Coma cluster according to [10]; *7* — core emission from 3C273 due to $p-\gamma$ interactions [11]; *8* — model [12] for the relativistic jet of 3C273 including $p-p$ and $p-\gamma$ interactions, and Supernova remnant gamma-Cygni (*9*) and IC 444 (*10*) according to [13]. The energy bounds on the AMANDA limit are restricted to the approximate region of sensitivity of the detector

The search for astrophysical sources of high-energy ($E_\nu > 1$ TeV) neutrinos is one of the central missions of the AMANDA detector. Figure 1 provides a survey of model predictions for the flux of high-energy neutrinos from point-like objects. It also contains the flux limit reported in this manuscript for sky bins with declinations greater than 30 degrees. Most theoretical models of potential astrophysical sources of neutrinos predict that the energy spectrum is very hard, approximately E^{-2} [5]. Due to the hard energy spectrum, the most probable energy of the detected neutrino is well above 1 TeV (typically 10–30 TeV).

In this report, we describe physics results obtained by the AMANDA detector. Due to the very nature of the experiment a classical calibration of the detector via an accelerator beam cannot be performed. It is thus very important to calibrate it with the «beam»

of atmospheric neutrinos. The observation of atmospheric neutrinos and detailed studies of down-going atmospheric muons have been used to study the sensitivity of the detector. The observed differences between observation and prediction are within ± 30 %, which is within the systematic uncertainty. After the point source analysis, we present the status of a general search for continuous emission from point sources in the Northern sky, restricted to declinations greater than $+5°$. Extraterrestic neutrinos can also arise from a diffuse flux. A first investigation on such a diffuse flux is presented. We also report preliminary results from a search for high-energy neutrinos from Gamma Ray Bursts (GRBs). Neutrino signals from GRBs should be correlated in direction and time, greatly simplifying background rejection. Low-energy neutrinos from burst-like events can also be detected. An analysis looking for signal from supernova explosions was performed. By restricting the atmospheric neutrino analysis to a search cone with a half angle of 15° about zenith, a search was made for neutrino emission from WIMP annihilation near the center of the Earth. Relativistic magnetic monopoles also emit Cherenkov radiation and a limit on their flux was calculated. Finally we present an analysis relating meteorological effects to AMANDA trigger rates via an effective temperature coefficient α_T. Unless stated otherwise, all results reported here are based on data collected between April and October of 1997. Due to limitations in the data acquisition and archiving system at that early phase of operation, the lifetime ranges between 130 and 140 days, depending on the details of the analysis.

1. ANALYSIS PROCEDURE — ATMOSPHERIC NEUTRINOS

The various physics objectives are best addressed by specialized analyses, although most are closely related. The search for atmospheric neutrinos can be used to illustrate the general methods. Trigger events are dominated by down-going atmospheric muons, so analysis techniques were developed to reject this background while retaining good efficiency for up-going neutrino-induced muons. Unlike many neutrino detectors, the effective sensitivity depends strongly on the background rejection requirements, which are considerably weaker for searches for point sources than for diffuse flux searches.

Monte-Carlo-based simulation programs determined the effective area for background and neutrino-induced muons. Several important results from these programs were tested by comparing the background simulation to the experimental data at various steps along the analysis chain.

Even after selecting events reconstructed as up-going, experimental data is dominated initially by background events — typically downward-going atmospheric muons with poorly known directions. This can be seen in Fig. 2 indicated by the flat behavior for less restrictive selection criteria (quality < 4.2). As selection criteria become progressively more restrictive (increasing values along the x axis), the asymptotic flattening of the ratio (experimental data)/(Signal MC atm ν) indicates that the evolution of the experimental data becomes consistent with signal expectation in the vicinity of the plot where the (BG MC)/Exp ratio approaches zero. From this evidence (and visual inspection), we conclude that the contamination in the atmospheric neutrino sample from known physics effects is small (< 15 %) for values of the event quality parameter greater than six. Background simulations with much greater statistical precision are currently underway.

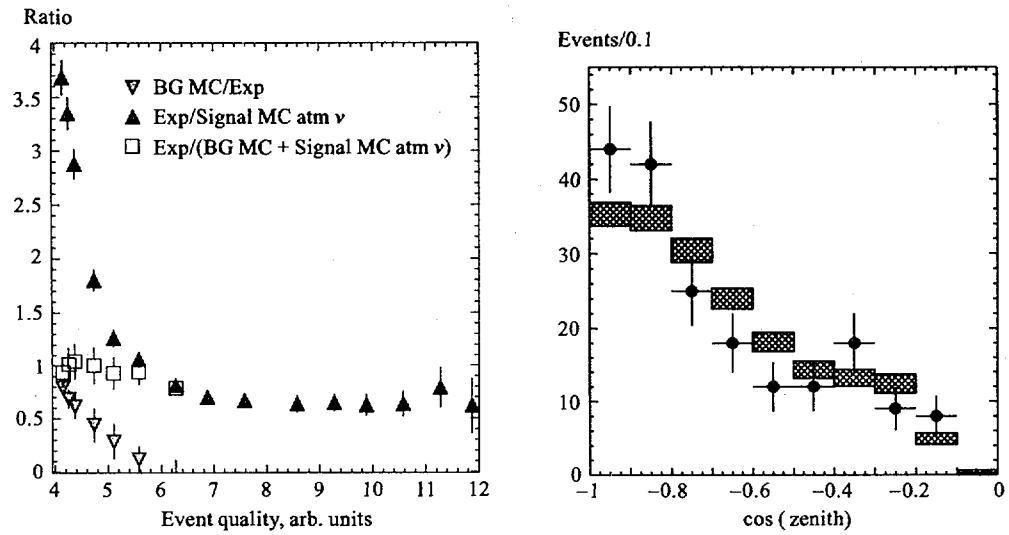

Fig. 2. Ratios of passing rates for simulated background (BG MC), simulated atmospheric neutrino signal (Signal MC atm ν), and reconstructed experimental data (Exp) as a function of «event quality», a variable which measures the severity of the selection criteria

Fig. 3. Reconstructed zenith angle distribution. The simulated atmospheric neutrino events (shaded boxes) are normalized to data (filled circles). The vertical widths of the boxes indicate the errors computed using binomial statistics

Figure 3 shows that the angular distribution of events is also consistent with the simulated distribution of atmospheric ν events. Due to the elongated cylindrical geometry of AMANDA-B10, the acceptance shows strong dependence on zenith angle. Thus, the angular dependence of the atmospheric neutrino sample is consistent with expectation and contamination from background is small. Finally, the distribution of the number of OMs in an event is also consistent with expectation (Fig. 9).

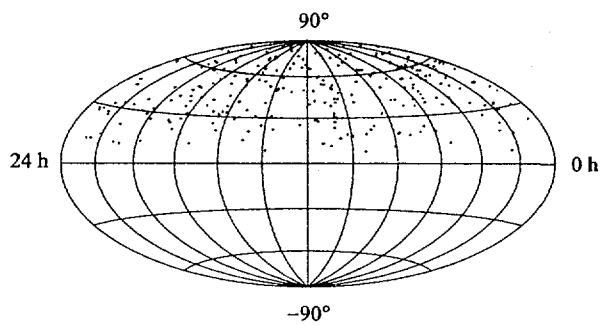

Fig. 4. Sky-plot in equatorial coordinates of the neutrino candidate events found by either of the two analyses

Due to the importance of the atmospheric muon analysis, two distinct analyses have been performed. Their results are consistent with each other and with simulation. A sky-plot of the combined sample of neutrino candidates can be seen in Fig. 4. As expected, no obvious clustering and no obvious void can be seen. Statistical tests show that the distribution is consistent with random fluctuations taking into account the non-uniform sensitivity in declination of the AMANDA array.

2. SEARCH FOR POINT SOURCES

The point source analysis procedure utilizes two essential characteristics of the signal to simplify the analysis relative to the atmospheric neutrino measurements. First, the sources are assumed to be point-like, so only events within a selected angular region in the sky are considered. Second, we use the topological characteristics of spectrally hard neutrino signal to reject poorly reconstructed atmospheric muons and atmospheric neutrinos, both having softer spectra. Topological variables include an estimate of muon energy and an assessment of the spatial fluctuation of the detected signals in a given event. The complete suite of variables was able to differentiate signal events from several classes of background topologies.

An iterative analysis procedure was developed to maximize $S/\sqrt{BG}$, where the signal, S, was computed with an energy spectrum proportional to E^{-2} for the source. BG is background from atmospheric muons and atmospheric neutrinos. After optimizing the analysis parameters, the sensitivity was evaluated for power law spectra with indices between 2.0 and 3.0.

The space angle resolution is determined from simulation. The upper panel of Fig. 5 shows that the median resolution is 3 degrees, and the lower panel indicates that this value only weakly depends on energy. Two studies were used to check the angular resolution and absolute offset. First, events that simultaneously trigger the GASP ACT [14] and AMANDA provide a «test beam» containing single muons with directional information provided by GASP. To improve the statistical accuracy of the investigation, a second study involved events which simultaneously trigger the SPASE air shower array [15] and AMANDA. Although the interpretation of these special events is complicated by the presence of multiple muons, which tend to reconstruct with worse angular precision than single muon events, the response of the detector to these events appears to be correctly modeled.

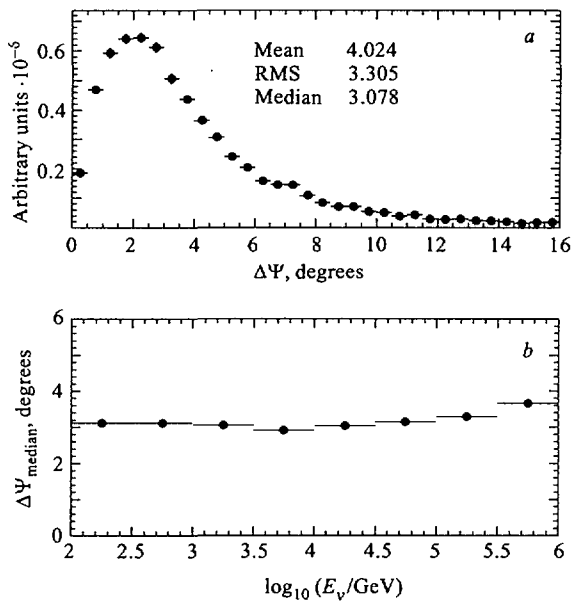

Fig. 5. Error in the space angle for simulated signal events with energy spectra proportional to E_ν^{-2}: (*a*) distribution of error averaged over declination; (*b*) space angle error as a function of neutrino energy

The point source analysis yields an event sample of 1097 events which are distributed on the sky as shown in Fig. 6.

Guided by the estimate of angular resolution, the sky was divided into 319 non-overlapping angular bins. The distribution of counts per sky bin is consistent with random fluctuations, which were determined by selecting all events within a declination band and randomly redistributing them in Right Ascension.

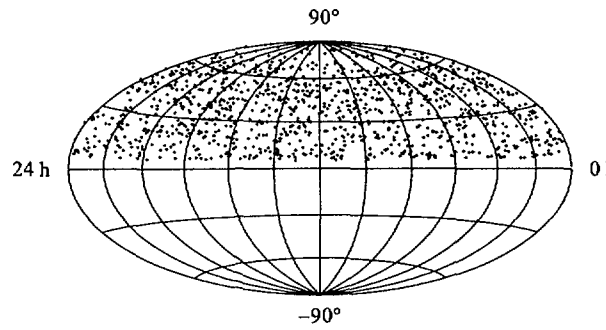

Fig. 6. Sky distribution of the 1097 events in the point source analysis. Coordinates are Right Ascension (RA) and declination (dec.). When looking for point sources, one does not optimize signal/noise. Instead, one is interested in signal/$\sqrt{\text{noise}}$ for optimal significance. Thus the sample used in this analysis is about 6 times larger than that in the atmospheric neutrino analysis in Fig. 4

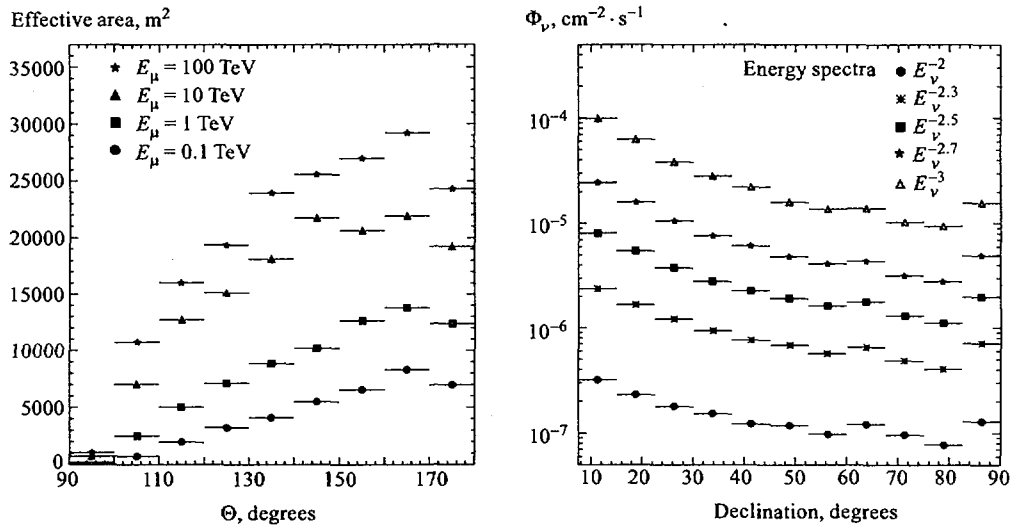

Fig. 7. The effective area for muon detection as a function of zenith angle for E_μ between 0.1 and 100 TeV (180° is vertically up in local detector coordinates)

Fig. 8. Preliminary neutrino flux limit (90 % C.L.) on point sources of high-energy neutrinos as a function of declination, averaged over RA. The limit is computed for a lower energy threshold of 10 GeV. Note that the power law exponent refers to the neutrino energy spectrum. Also, neutrino absorption by the Earth is taken into account

The neutrino limits were computed according to

$$\phi_\nu^{\text{limit}}(E_\nu > E_\nu^{\min}) = \frac{\mu(N_b, N_0)}{T_{\text{live}}\epsilon\overline{A}_{\text{eff}}^{\nu}}\,, \tag{1}$$

where $\overline{A}_{\text{eff}}^{\nu}$ is the neutrino effective area weighted by the assumed neutrino energy spectrum.

This quantity is related to the muon effective area shown in Fig. 7. The factor $T_{\rm live}$ is the lifetime of the experiment. The term ϵ is the efficiency due to finite angular resolution and also accounts for non-central source placement within an angular search bin. The term $\mu(N_b, N_0)$ generates the 90 % confidence limit according to Feldman and Cousins [16] for signal events given the measured number of events in the search bin, N_0, and the expected background N_b determined from the events in the declination band containing the source bin. The results of this calculation are shown in Fig. 8 for various assumed spectral indices of the initial neutrino flux.

The inferred limits on neutrino flux apply to point sources with continuous emission (or episodic emission averaged over a time interval of approximately 0.6 years) and power law energy spectra with a fixed spectral index above the energy threshold of the detector. The limits for sources at large positive declination are comparable to the best published limits in the Southern sky [17].

3. HIGH-ENERGY DIFFUSE FLUX

Many models of diffuse emission from unresolved sources predict an energy spectrum that is much harder than the atmospheric neutrino spectrum. Therefore, a limit on the diffuse flux can be extracted by searching for an excess of events at large energies. A simple, although not very precise, measure of energy of the neutrino-induced muons is counting the number of hit channels — optical modules that detected Cherenkov light. Figure 9 shows the distribution of the hit multiplicity for experimental data, for simulated atmospheric neutrinos, and for an arbitrarily normalized, relatively hard (E^{-2}) energy spectrum. The experimental data agree with the atmospheric neutrino spectrum. From the non-observation of an excess of high multiplicity events, we derive an upper limit on an assumed diffuse E^{-2} spectrum. The preliminary limit (90 % C.L.) is of order $dN/dE_\nu \leq 10^{-6} E_\nu{}^{-2} \mathrm{cm}^{-2}\cdot\mathrm{s}^{-1}\cdot\mathrm{sr}^{-1}\cdot\mathrm{GeV}^{-1}$. This experimental limit is below some models (e.g., [11]), but still above the recent model-independent bound established by Waxman and Bahcall [18]. The experimental limit can be improved by developing better energy estimators using charge and topological hit information. The response of the detector to muons with energies in excess of 100 TeV is still under investigation.

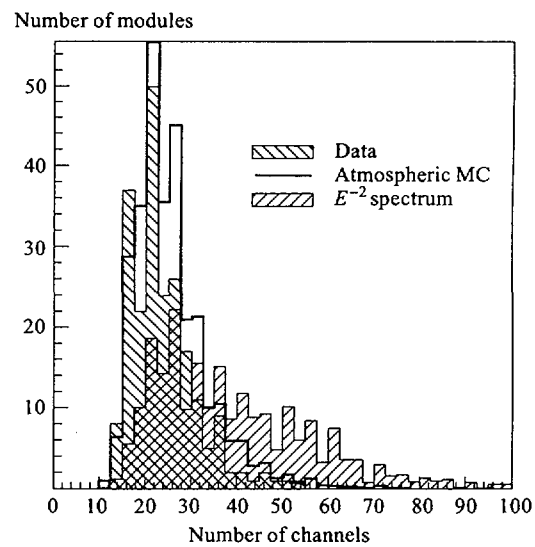

Fig. 9. Distribution of the number of optical modules for the data presented in Fig. 3. The MC simulations for atmospheric neutrinos and a generic spectrum $10^{-5} E^{-2}\,\mathrm{cm}^{-2}\cdot\mathrm{s}^{-1}\cdot\mathrm{sr}^{-1}\cdot\mathrm{GeV}^{-1}$ are also shown

4. GRB SEARCH

Gamma Ray Bursts (GRBs) are thought to be produced by highly relativistic outflows originating from a compact, explosive event. A search for emission of high-energy neutrinos correlated in time and direction with GRBs was performed. We examined a total of 78 GRBs detected by BATSE. The T_{90} duration of the bursts, defined as the time required to accumulate between 5 and 95 % of the total counts, varied between 0.2 and 200 s. Guided by several models for neutrino emission [19,20], the analysis procedure optimized the effective area of the AMANDA detector for neutrino energies between 100 TeV and 1 PeV. The lack of a statistically significant excess from any GRB examined in 1997 leads to a range of limits (the variation is primarily due to neutrino attenuation by the Earth which depends on arrival direction) on the fluence that span from $E_\nu^2 dN/dE_\nu \leq 0.05 \div 0.1 \min(1, E_\nu/E_{\rm break})\,{\rm TeV\cdot cm^{-2}}$ (Fig. 10).

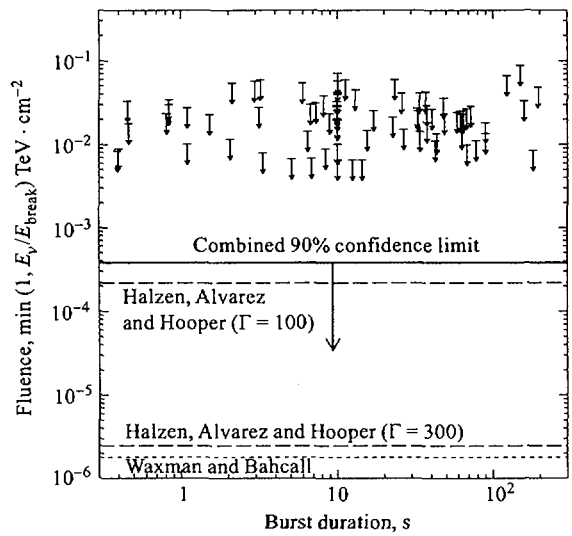

Fig. 10. Individual and combined limits on GRB fluence obtained from 78 GRBs. Theoretical predictions [19,22] are plotted for comparison

The parameter $E_{\rm break}$, which is of order 500 TeV, is the energy that characterizes the change in the power law of neutrino spectrum (approximately E^{-1} for $E_\nu < E_{\rm break}$ and E^{-2} for neutrinos with energies larger than $E_{\rm break}$. Another change in the spectral index is expected at even higher energies, but this feature does not impact on our analysis. Using all of the GRBs, a preliminary cumulative upper limit of $E_\nu^2 dN/dE_\nu \leq 4 \cdot 10^{-4} \min(1, E_\nu/E_{\rm break})\,{\rm TeV\cdot cm^{-2}}$ was derived [21]. For comparison, Waxman and Bahcall [19] predict a fluence of $E_\nu^2 dN/dE_\nu \leq 4.8 \cdot 10^{-7} \min(1, E_\nu/E_{\rm break})\,{\rm TeV\cdot cm^{-2}}$.

5. SUPERNOVA SEARCH

The standard AMANDA operation mode is aimed at detecting and reconstructing long muon tracks. However, monitoring of a huge ice volume permanently with a few hundred

PMTs also allows one to search for bursts that follow energy neutrinos, originating, e.g., from gravitational stellar collapses. Supernova (SN) neutrinos which interact inside the detector close enough to a given PMT will cause an enlarged counting rate for the duration of the SN neutrino burst (typically 10 s).

Once these «noise» rate changes are sampled with a large number of PMTs, coherent fluctuations much smaller than one standard deviation per PMT become significant. Such an SN search with the AMANDA detector, as proposed by [24], would detect the dominant reaction channel $\overline{\nu}_e + p \rightarrow e^+ + n$ with the positron's Cherenkov light triggering a PMT. The effective detection volume $V_{\rm eff}$ per optical module is determined by the optical properties of the ice, and is calculated to be $V_{\rm eff} \approx 410\,{\rm m}^3$ [23]. An SN of the same luminosity as SN1987A, located at the center of our galaxy (8.5 kpc distance), would yield about 100 counts per PMT. Typical noise rates in AMANDA are around 320 Hz or around 1.1 kHz, depending on the K-40 contamination in the OM glass batch.

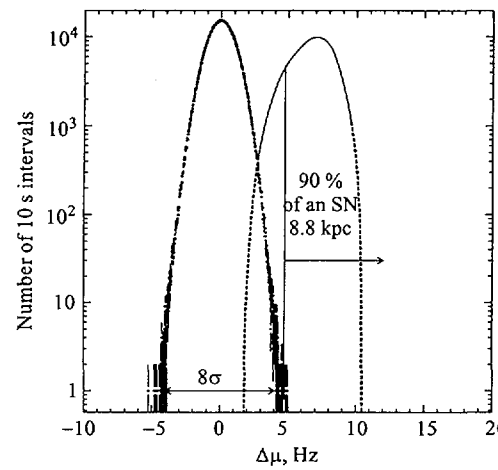

Fig. 11. 1997 & 1998 data (left distribution) compared to an equivalent data set simulated for SN1997-A type signals. 90 % of a Supernova neutrino burst located at 8.8 kpc distance would be seen above a cut for less than one fake event per year (vertical line)

The background to this signal is determined by the noise fluctuations of all PMTs. Due to strict quality criteria, we analyzed only a subset of very stable PMTs (stable noise rates) over 219.7 days effective lifetime for 1997 and 1998. The results can be seen in Fig. 11. An SN signal detected with 90 % efficiency at a distance of 8, 4, 2 and 1 kpc would correspond to a significance of 5, 7, 23.3, 93 and 372 standard deviations respectively.

6. WIMP SEARCH

There is strong evidence for a non-baryonic component in the dark matter in the Universe. Supersymmetric extensions to the Standard Model provide promising dark matter candidates, such as the neutralino. Dark matter in the galactic halo can interact with nuclei in the Earth, loose energy and become trapped. The annihilation of neutralinos within the core of the Earth will generate high-energy neutrinos in the nearly vertical direction ($\cos\theta < -0.97$). For this highly restricted search cone, the number of events observed agrees with prediction (17 predicted, 15 observed). Therefore, the lack of a statistically significant excess of neutrino events in the nearly vertical direction can be used to constrain the flux of neutrinos from neutralino annihilation.

Figure 12 compares the AMANDA limits with predictions [25] for a broad class of supersymmetric models, and with curves derived [26] from published limits by MACRO [17] and Baksan [27], illustrating the potential of the technique. Systematic errors associated with

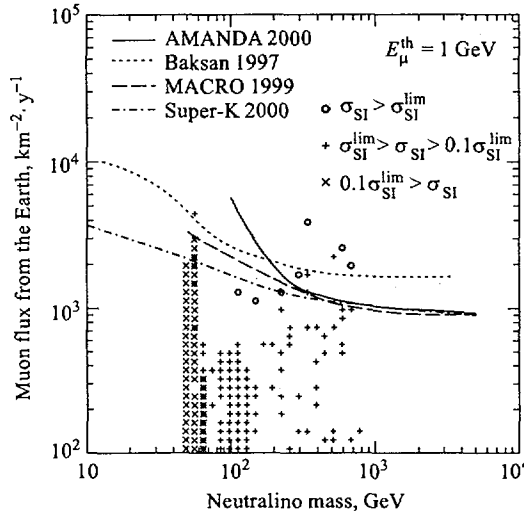

Fig. 12. High-energy muon flux predictions and experimental limits due to the annihilation of supersymmetric particles in the center of the earth. See Ref. 25 for explanation of symbols. The AMANDA limit (90 % C.L.) was corrected to correspond to a threshold of 1 GeV

detector sensitivity and neutrino oscillation physics are currently under investigation, but are expected to weaken the limits.

7. MAGNETIC MONOPOLES

In 1931, P.A.M.Dirac showed that adding magnetic charge and current terms to the Maxwell equations and requiring gauge invariance and single-valuedness of the wave function lead to a minimum magnetic charge of $q_m = 1/2\alpha \approx 137/2e$ [28]. Forty-three years later 't Hooft established monopoles within the framework of GUTs [29] which required the creation of monopoles in the early Universe at the time of the GUT phase transition. It has been discussed whether the highest energy cosmic rays do consist of magnetic monopoles of mass $\sim 10^{10}$ GeV, accelerated by the galactic fields ($\sim 10^{-6}$ G) [30].

A monopole passing through the AMANDA detector would cause very high light output (8300 times that of a μ [31] at a velocity $\beta \approx 1$) which again would lead to many PMTs hit. The search for such bright events is thus the basic principle of monopole detection. The main background contamination arises from atmospheric showers, which produce bright muon bundles in the detector.

In order to discriminate against this background, again only events reconstructed as upgoing were analyzed. Figure 13 shows the resulting flux limits for various values of β. Upper limits range from $3.6 \cdot 10^{-16}$ (at $\beta = 0.8$) to $1.5 \cdot 10^{-16}$ cm^{-2}·s^{-1}·sr^{-1} (at $\beta = 1.0$). Only one measurement [33] achieves a lower upper limit, using the current induced in a superconducting coil by monopoles trapped in lunar rock. Whereas that method makes assumptions on the formation of the moon's surface, our value is based on the direct (non-)observation of a moving monopole.

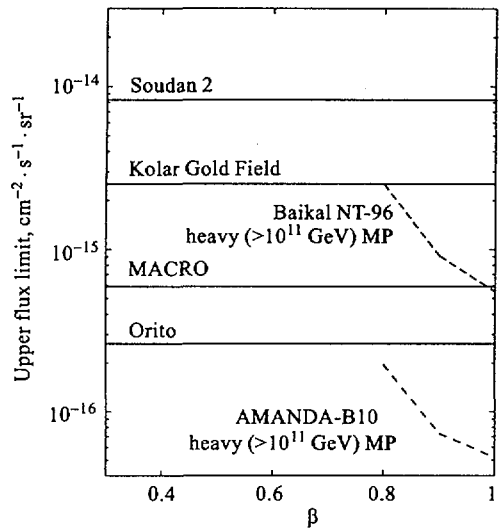

Fig. 13. Upper flux limit (90 % C.L.) for various experiments versus the monopole velocity. Taken from [32]

8. SEASONAL VARIATIONS

Atmospheric muons are produced in the decay of charged pions and kaons, which are themselves the results of the interaction of cosmic rays with air. It is expected that their flux is affected by atmospheric variations [34–36]. At the high atmospheric muon energies (> 500 GeV at the surface level) capable of triggering the AMANDA detector, the main effect that can be seen is due to the competition between interaction and decay of the parent particles. A temperature rise between the layer where these particles are produced (≈100 mbar) and the one where they interact (≈200 mbar) leads to a lower atmospheric density and to a larger fraction of them decaying into muons. Therefore, the muon intensity is expected to be of the low temperature fluctuations.

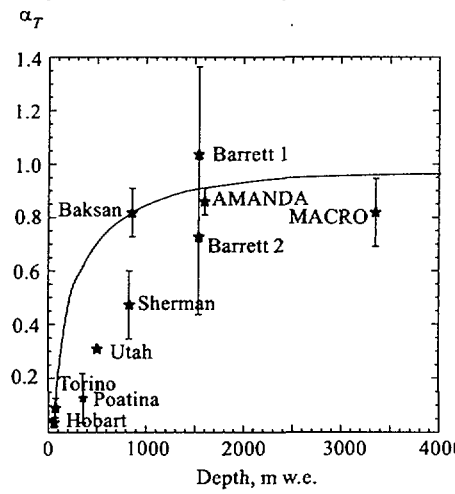

Fig. 14. Measurements of α_T by detectors at different depths, with the expected curve and with AMANDA value added (From [35])

Detailed weather data are collected via daily balloon flights and made available by the Antarctic Meteorology Research Center. Given the high quality of the meteorological data and the specific conditions prevailing at the South Pole (no 24-hour cycle, large temperature differences between summer and winter), it is of interest to search for correlations between the trigger rate recorded by AMANDA and the meteorological variations.

The temperature effect at high energy is described by [37]

$$\frac{\Delta I_\mu}{I_\mu^0} = \int_0^\infty dX \alpha(X) \frac{\Delta T(X)}{T(X)} , \tag{2}$$

where I_μ is the muon intensity above the detector energy threshold, ΔI_μ is the fluctuation around a nominal intensity I_μ^0, $\alpha(X)$ is the temperature coefficient and $\Delta T(X)$ and $T(X)$ are the temperature fluctuation and temperature at a given atmospheric depth X. The integration is performed across the whole atmosphere. As discussed in [35], an effective temperature $T_{\rm eff}$ can be defined to replace equation (2) by

$$\frac{\Delta R_\mu}{\langle R_\mu^0 \rangle} = \alpha(X) \frac{\Delta T_{\rm eff}(X)}{\langle T_{\rm eff}(X) \rangle}. \tag{3}$$

Fitting the relative trigger rate to the relative variation of $T_{\rm eff}$, taking into account the errors on both variables, we get $\alpha_T = 0.86 \pm 0.05$, as can be seen from Fig. 14.

Acknowledgements. This research was supported by the U.S. National Science Foundation Office of Polar Programs and Physics Division, the University of Wisconsin, Alumni Research Foundation, the U.S. Department of Energy, the Swedish Natural Science Research Council, the Swedish Polar Research Secretariat, the Knut and Alice Wallenberg Foundation, Sweden, the German Ministry for Education and Research, the U.S. National Energy Research Scientific Computing Center (supported by the Office of Energy Research of the U.S. Department of Energy), UC-Irvine AENEAS Supercomputer Facility, Deutsche Forschungsgemeinschaft (DFG). C.P.H. received support from the EU 4th framework of Training and Mobility of Researchers, contract ERBFMBICT91551 and D.F.C. acknowledges the support of the NSF CAREER program. P.L. was supported by grant from the Swedish STINT program. P.D. was supported by the Körber Foundation.

REFERENCES

1. See contributions: Proc. of the 26th Intern. Cosmic Ray Conf. (ICRC99), Salt Lake City, UT, Aug. 1999. HE 3.1.06, HE 6.3.07, HE 4.2.06, HE 6.3.01, HE 4.1.15, HE 5.3.05, HE 4.2.05, HE 6.3.02, HE 4.1.14, HE 4.1.14, HE 3.2.11, HE 4.2.07, HE 5.3.06.
2. *Wischnewski R. et al.* // Nucl. Phys. A (Proc. Suppl.). 1999. V. 75. P. 412–414.
3. *Barwick S.W.* (AMANDA collaboration) // Nucl. Phys. B (Proc. Suppl.). 2000. V. 87. P. 402.
4. *Andres E. et al.* // Astropart. Phys. 2000. V. 13. P. 1–20.
5. *Stecker F.W., Salamon M.H.* // Space Sci. Rev. 1996. V. 75. P. 341–355; *Rachen J.P., Meszaros P.* // Phys. Rev. D. 1998. V. 58. P. 123005; Proc. of High Energy Neutrino Astrophysics Workshop (U. Hawaii). Singapore.
6. *Learned J.G., Mannheim K.* // Ann. Rev. Nucl. Part. Phys. 2000. (To appear).
7. *Agrawal V.* // Phys. Rev. D. 1996. V. 53. P. 1314.
8. *Nellen L., Mannheim K., Biermann P.L.* // Phys. Rev. D. 1993. V. 47. P. 5270.
9. *Bednarek W., Protheroe R.J.* // Mon. Not. Roy. Astro. Soc. 1997. V. 287. P. 560.
10. *Colafrancesco S., Blasi P.* // Astropart. Phys. 1998. V. 9. P. 227.

11. *Stecker F.W., Salamon M.H.* // Sp. Sci. Rev. 1996. V. 75. P. 341.
12. *Mannheim K.* // Phys. Rev. D. 1993. V. 48. P. 2408.
13. *Gaisser T.K., Protheroe R.J., Stanev T.* // Ap. J. 1998. V. 492. P. 219.
14. *Barbagli G. et al.* // Nucl. Phys. B (Proc. Suppl.). 1993. V. 32. P. 156.
15. *Dickinson J.E. et al.* // Nucl. Instr. Meth. A. 2000. V. 440. P. 95.
16. *Feldman G.J., Cousins R.D.* // Phys. Rev. D. 1998. V. 57. P. 3873.
17. *Montaruli T. et al.* // Proc. of the 26th ICRC. 1999. HE 4.2.03; *Ambrosio M. et al.* Submitted to «Astrophys. J.». 2000; astro-ph/0002492.
18. *Waxman E., Bahcall J.N.* // Phys. Rev. D. 1999. V. 59. P. 023002.
19. *Waxman E., Bahcall J.* // Phys. Rev. Lett. 1997. V. 78. P. 2292.
20. *Halzen F., Jaczko G.* // Phys. Rev. D. 1996. V. 54. P. 2774.
21. *Bay R.* Ph.D dissertation, Univ. of California-Berkeley, 2000. astro-ph/0008255.
22. *Alvarez-Muniz J., Halzen F., Hooper D.W.* astro-ph/0006027. To be published in «Phys. Rev. D».
23. *Jacobsen J.E.* Ph. D Thesis, Univ. Madison, 1996.
24. *Halzen F., Jacobsen J.E., Zas E.* // Phys. Rev. D. 1994. V. 29. P. 1758.
25. *Bergstrom L., Edsjo J., Gondolo P.* // Phys. Rev. D. 1998. V. 58. P. 103519; hep-ph/9806293.
26. *Edsjo J.* Private communication, 2000.
27. *Boliev M.M. et al.* // Nucl. Phys. B (Proc. Suppl.). 1996. V. 48. P. 83.
28. *Dirac P.A.M.* // Porc. Roy. Soc. A. 1931. V. 133 P. 60.
29. *t'Hofft G.* // Nucl. Phys. B. 1974. V. 79. P. 276–284.
30. *Kephart T.W., Weiler T.J.* // Astropart. Phys. 1996. V. 4. P. 271–279; *Escobar C.O., Vaszquez R.A.* // Astropart. Phys. 1999. V. 10. P. 197–202.
31. *Jackson J.D.* Classical Electrodynamics. New York, 1962, 1975.
32. *Cei F.* (MACRO collaboration). hep-ex/9810012, 1998.
33. *Alvarez et al.* // Science. 1970. V. 167. P. 701.
34. *Allkofer O.C.* Introduction to Cosmic Radiation. Verlag Karl Thiemig, 1975.
35. *Ambrosio M. et al.* (MACRO collaboration) // Astropart. Phys. 1997. V. 7. P. 109–124.
36. *Andreyev Yu.N.* // Proc. of the 21st ICRC, Adelaide, 1990. SH 8.2-10.
37. *Barrett K. et al.* // Rev. Mod. Phys. 1952. V. 24. P. 133.

The AMANDA collaboration includes: E.Andres[8], P.Askebjer[4], X.Bai[1], G.Barouch[8], S.W.Barwick[6], R.C.Bay[5], K.-H.Becker[13], L.Bergström[4], D.Bertrand[10], A.Biron[2], J.Booth[6], O.Botner[11], A.Bouchta[2], M.M.Boyce[8], S.Carius[3], D.Chirkin[5,13], J.Conrad[11], C.G.S.Costa[10], D.F.Cowen[7], J.Dailing[6], E.Dalberg[4], T.De Young[8], P.Desiati[2], J.-P.Dewulf[10], P.Doksus[8], J.Edsjö[4], P.Ekström[4], B.Erlandsson[4], T.Feser[12], M.Gaug[2], A.Goldschmidt[9], A.Goobar[4], H.Haase[2], A.Hallgren[11], F.Halzen[8], K.Hanson[7], R.Hardtke[8], Y.D.He[5], M.Hellwig[12], H.Heukenkamp[2], G.C.Hill[8], P.O.Hulth[4], S.Hundertmark[6], J.Jacobsen[9], A.Karle[8], J.Kim[6], B.Koci[8], L.Köpke[12], M.Kowalski[2], H.Leich[2], M.Leuthold[2], P.Lindahl[3], I.Liubarsky[8], P.Loaiza[11], D.M.Lowder[5], J.Ludvig[9], J.Madsen[8], P.Marciniewski[11], H.Matis[9], T.Mikolajski[2], T.C.Miller[1], Y.Minaeva[4], P.Miocinovic[5], P.Mock[6], R.Morse[8], T.Neunhöffer[12], F.M.Newcomer[7], P.Niessen[2], D.R.Nygren[9], C.Pérez de los Heros[11], R.Porrata[6], P.B.Price[5], K.Rawlins[8], C.Reed[6], W.Rhode[13], A.Richards[5], S.Richter[2], J.Rodriguez Martino[4], P.Romenesko[8], D.Ross[6], H.Rubinstein[4], H.-G.Sander[12], T.Scheider[12], T.Schmidt[2], D.Schneider[8], E.Schneider[6], R.Schwarz[8], A.Silvestri[2,13], M.Solarz[5], G.Spiczak[1], C.Spiering[2], N.Starinski[8], D.Steele[8], P.Steffen[2], R.G.Stokstad[9], O.Streicher[2], Q.Sun[4], I.Taboada[7], L.Thollander[4], T.Thon[2], S.Tilav[8], M.Vander Donckt[10], C.Walck[4], C.Weinheimer[12], C.H.Wiebusch[2], R.Wischnewski[2], K.Woschnagg[5], W.Wu[6], G.Yodh[6], S.Young[6].

[1] Bartol Research Institute, University of Delaware, Newark, DE 19716 USA

[2] DESY-Zeuthen, D-15735, Zeuthen, Germany

[3] Dept. of Technology, University of Kalmar, S-39129, Kalmar, Sweden

[4] Dept. of Physics, Stockholm University, S-11385, Stockholm, Sweden

[5] Dept. of Physics, University of California, Berkeley, CA 94720 USA

[6] Dept. of Physics and Astronomy, University of California, Irvine, CA 92697 USA

[7] Dept. of Physics and Astronomy, University of Pennsylvania, Philadelphia, PA 19104 USA

[8] Dept. of Physics, University of Wisconsin, Madison, WI 53706 USA

[9] Lawrence Berkeley National Laboratory, Berkeley, CA 94720 USA

[10] Brussels Free University, B-1050, Brussels, Belgium

[11] Dept. of Radiation Sciences, University of Uppsala, S-75121, Uppsala, Sweden

[12] Institute of Physics, University of Mainz, D-55099, Mainz, Germany

[13] Fachbereich 8 Physik, BUGH Wuppertal, D-42097, Wuppertal, Germany